



# OPEN The role of RNA structural motifs in RNA-lipid raft interaction

Rafał Mańka<sup>1</sup>, Karolina Sapoń<sup>1,3</sup>, Joanna Zaziąbło<sup>1</sup>, Teresa Janas<sup>1</sup>, Aleksander Czogalla<sup>2</sup> & Tadeusz Janas<sup>1</sup>✉

Here, we sought to determine the role of specific RNA structural motifs in the interaction of RNA with model lipid vesicles containing liquid-ordered domains (RAFT liposomes). We show that the presence of several small apical loops within RNA structure favors RNA affinity for RAFT liposomes while the increased number of nucleotides within bulges inhibits this affinity. FRET flow cytometry measurements confirmed a modulation of the interaction of RNA with plasma membrane by the presence of specific RNA structural motifs. The analysis of viral RNA fragments revealed that a long double helix at the apical loop increases the affinity of viral RNA to lipid rafts. The analysis of exosomal Y RNAs secreted by nematode parasites showed that the presence of the EXO-motif GGAG is strongly correlated to the presence of small number of large apical loops within RNA structure. These results show that RNA structural motifs can modulate RNA affinity to liquid-ordered membrane lipid raft domains thus suggesting the importance of these motifs both for the mechanism of RNA loading into extracellular vesicles, and for the development of RNA-based lipid biosensors for monitoring of viral RNAs in biofluids and wastewater.

**Keywords** Dissociation constant, Flow cytometry, Lipid rafts, Membranes, RNA, Structural motifs

In recent years, extracellular vesicles, particularly exosomes, have garnered significant interest<sup>1–3</sup>. Composed of a lipid bilayer and membrane proteins, exosomes are produced in endosomal compartments within multivesicular bodies (MVBs). They mediate cell signaling by transporting molecules such as nucleic acids, proteins, and lipids produced in cells<sup>4–6</sup>. Exosome-transported RNAs play a crucial role in regulating biological processes in both health and disease. Exosomal miRNAs facilitate intercellular communication over short and long distances, influencing various physiological and pathological processes via paracrine and endocrine pathways<sup>7</sup>. In physiological conditions, exosomal miRNAs participate in cellular communication, such as in immunological synapses or in the cardiovascular system. In cancer, exosomal miRNAs can be delivered to recipient cells within the tumor microenvironment or to distant sites in the body, influencing gene expression regulation to promote angiogenesis and metastasis<sup>8</sup>.

Similar RNA types have been found in vesicles from various cell types, suggesting a common mechanism for selectively loading RNA into exosomes. Attempts have been made to elucidate this process. Apart from mechanisms involving protein complexes, particularly endosomal sorting complexes required for transport (ESCRT)<sup>9,10</sup>, there are hypotheses suggesting direct interaction between RNA molecules and vesicle membranes. In this context, the properties of lipids in the inner membrane layer are thought to influence vesicle formation and RNA loading<sup>11–14</sup>. These processes investigate properties such as lipid rafts in multivesicular body membranes or RNA characteristics.

Membrane rafts are small, heterogeneous, highly dynamic, sterol- and sphingolipid-enriched domains that participate in various cellular processes<sup>15</sup>. Compared to the rest of the membrane, raft domains have more densely packed lipids with higher cholesterol and glycolipid content. Cholesterol is present in both raft (ordered) and non-raft membrane fractions, with ordered areas containing over 40% cholesterol<sup>16</sup>. The fatty acid chains in rafts are longer and more saturated than those in non-raft membranes. The van der Waals interactions between saturated fatty acid chains of sphingolipids and cholesterol are crucial for raft formation<sup>14,17–19</sup> although hydrogen bond linking the hydroxyl group of cholesterol and the amide group of sphingolipids also play important role.

RNA, with its 2'OH group, has an intrinsic ability to form complex spatial structures. The high frequency of 2'OH group binding to another 2'OH or a phosphate backbone suggests that these hydrogen bond interactions may be sequence-independent in these regions, although the overall secondary structure of RNA depends on the sequence<sup>20</sup>. RNA folding involves double-stranded fragments formed by base pairing and remaining single-

<sup>1</sup>Institute of Biology, University of Opole, Kominka 6, 45-032 Opole, Poland. <sup>2</sup>Department of Cytochemistry, Faculty of Biotechnology, University of Wrocław, F. Joliot-Curie 14a, 50-383 Wrocław, Poland. <sup>3</sup>Karolina Sapoń is deceased. ✉email: tadeusz.janas@uni.opole.pl

stranded fragments. The basic motifs of RNA secondary structure include stems, bulges, internal loops, apical loops, and single-stranded terminal regions<sup>21</sup>.

In our previous article<sup>22</sup>, we analyzed interactions of certain RNA oligonucleotides with ordered and disordered vesicle membranes. The results indicated that RNAs can directly interact with lipid membranes, and the presence of raft domains promotes RNA affinity for lipid vesicle membranes. Here, we continue this study by assessing the role of RNA structure in RNA-membrane interactions. Specifically, we investigate whether particular structural motifs in RNA facilitate its interaction with RAFT vesicles.

## Results

### Measurements of RNA interaction with lipid vesicles

To assess the role of RNA structural motifs in RNA-membrane interactions, the affinity levels of 13 different RNA aptamers and 6 different RNA fragments of HTLV-1 to RAFT liposomes has been measured (Supplementary Tables S1 and S4). As the main criterion for selecting the RNA aptamer pool we have chosen to obtain various combinations of RNA sequence motifs in various locations (see Materials and Methods). In addition, measurements of  $K_D$  for RNA aptamers to DOPC liposomes has been performed (Supplementary Table S1). The fluorescence measurements were based on RNA-to-membrane FRET between RNA-bound YOYO-1 (donor) and membrane-bound LissRh-PE (acceptor)<sup>23</sup>. At RNA titration with liposomes, a decrease in YOYO-1 fluorescence was observed, indicating energy transfer from RNA-bound YOYO-1 (donor) to liposome-bound LissRh-PE (acceptor), triggered by the RNA-lipid membrane interaction. Based on the fluorescence changes of the donor, the  $K_D$  values were calculated for each measurement. Supplementary Table S1 shows the obtained average  $K_D$  values for the particular RNAs measured.

### Analysis of RNA aptamers structural motif

Using the Mfold program<sup>24</sup>, the secondary structures of the tested RNAs have been predicted. The analyses refer to the proposed secondary structure with the lowest free energy among the given structural variants. If any alternative structural variants existed, they are listed in the Supplementary Table S2. The free energy difference between the first and second proposed structures typically ranges from 0 to 1.3 kcal/mol, with an average difference of 0.5 kcal/mol. Because the energies involved in the formation of secondary structure are larger than those involved in tertiary interactions, secondary structural elements can exist and be stable by themselves<sup>25</sup>, not being disturbed by RNA-membrane interactions. In the predicted folding of the RNA oligonucleotides, the following secondary structure motifs are marked: double helix, bulge, internal loop, multi-branch loop, apical loop, and single-stranded terminal regions at the molecule's ends (Supplementary Table S1).

To determine the importance of secondary structure motifs in RNA-membrane interactions, a correlation analysis has been performed between the obtained average  $K_D$  values and the percentage of nucleotides in particular structural motifs (Fig. 1.A, Supplementary Fig. S1). The calculated Spearman's correlation coefficient shows a relatively strong correlation between the  $K_D$  value and the occurrence of bulges, indicating that this motif may be involved in RNA-membrane interactions (Fig. 1.A). This observation indicates that the increased number of nucleotides within bulges inhibits RNA affinity for RAFT membranes. The increased number of nucleotides within bulges can result from the increased number of bulges and/or increased size of bulges.

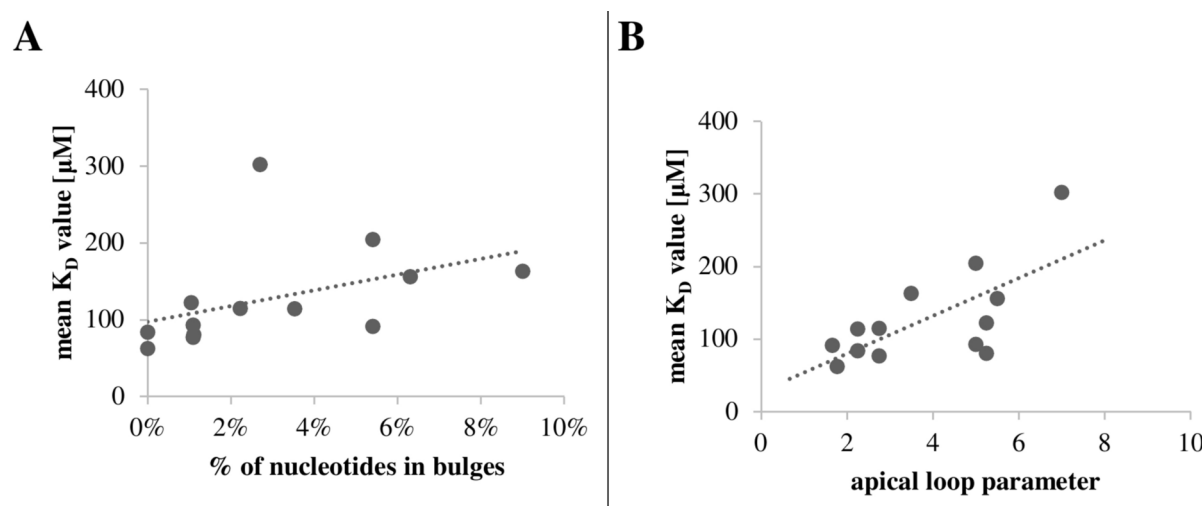


**Fig. 1.** (A) Correlation of mean  $K_D$  value and the percentage of nucleotides in bulges for RNA-RAFT liposome complexes. The correlation analysis is performed with the determination of Spearman's correlation coefficient, equal to 0.7, and the statistical significance is tested for a p-value of 0.05 ( $r_s = 0.70$ ,  $n = 13$ ). (B) Correlation of mean  $K_D$  value and the apical loop parameter. An apical loop parameter is calculated as the ratio of the average number of nucleotides per an apical loop to the number of apical loops for each analyzed RNA ( $n = 13$ ). The calculated Spearman's correlation coefficient equals to 0.64, with statistical significance for a p-value of 0.05 ( $n = 13$ ). Sequences of RNA aptamers were folded using the Mfold program<sup>24</sup> at a set temperature of 37 °C.

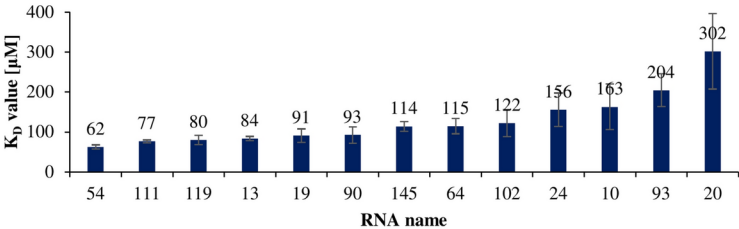
Additionally, for each RNA, the apical loop parameter has been calculated as the ratio of the average number of nucleotides per apical loop to the number of apical loops. The value of the apical loop parameter increases with the increase of size of the apical loop and the decrease of the number of loops. Figure 1.B shows the correlation between the average  $K_D$  value and this parameter. A positive correlation with a coefficient equal to 0.68 is obtained showing that the  $K_D$  value increases (i.e. the affinity decreases) as the size of the apical loop increases or/and the number of loops decreases. These observations indicate that the presence of several small apical loops within RNA structure favors RNA affinity for RAFT membranes. A correlation analysis between the obtained average  $K_D$  values and the percentage of nucleotides in other structural motifs (including stems, multi-branch loops, apical loops, internal loops, single-stranded terminal regions) shows no statistical significance. These results are included in Supplementary material (Supplementary Figure S1). A correlation analysis between the obtained average  $K_D$  values for RNA aptamers-DOPC liposome complexes (Supplementary Table S1) and structural motifs (including apical loop parameter, the percentage of nucleotides in stems, bulges, multi-branch loops, apical loops, internal loops, single-stranded terminal regions) shows no statistical significance (Supplementary Figure S2).

We have also applied an alternative structural prediction method (RNAfold program) for RNA aptamers (Supplementary Table S3). A correlation analysis between the obtained average  $K_D$  values for RNA aptamers-RAFT liposome complexes and the percentage of nucleotides in bulges as well as between the obtained average  $K_D$  values and the apical loop parameter shows statistical significance (Supplementary Figure S3) thus validating the results obtained using Mfold program.

We can analyze RNA 111 structure (Supplementary Table S1) as an example of the potential impact of small apical loops on RNA-membrane interactions. RNA 111 has the second-strongest affinity for RAFT membranes, with  $K_D = 77 \pm 4 \mu\text{M}$  (Fig. 2). The predicted secondary structure of this RNA contains two distinct apical loops (nucleotides 26–40 and 70–75) with a small 5 (and 6)-nucleotide loops and a five (and three) base pair long stem. This arrangement of a small apical loops on stable stems may increase RNA-membrane affinity. On the contrary, the weakest affinity for RAFT vesicles is shown by RNA 20 ( $K_D = 302 \pm 94 \mu\text{M}$ ) (Fig. 2, Supplementary Table S1). The secondary structure of RNA contains the longest (37-nucleotide) single-stranded terminal region at the 3' end (nucleotides 83–86). This result suggests that the presence of a long single-stranded terminal reduces RNA-membrane interactions. Interestingly, this RNA is the only one among the analyzed oligonucleotides that shows stronger affinity for LUV<sub>DOPC</sub> membranes ( $K_D = 141 \pm 9 \mu\text{M}$ ) rather than LUV<sub>RAFT</sub> ( $K_D = 302 \pm 94 \mu\text{M}$ ), suggesting that the presence of this long single-stranded 3' ending does not disturb RNA interaction with the disordered membrane to the same extent as the ordered membrane.

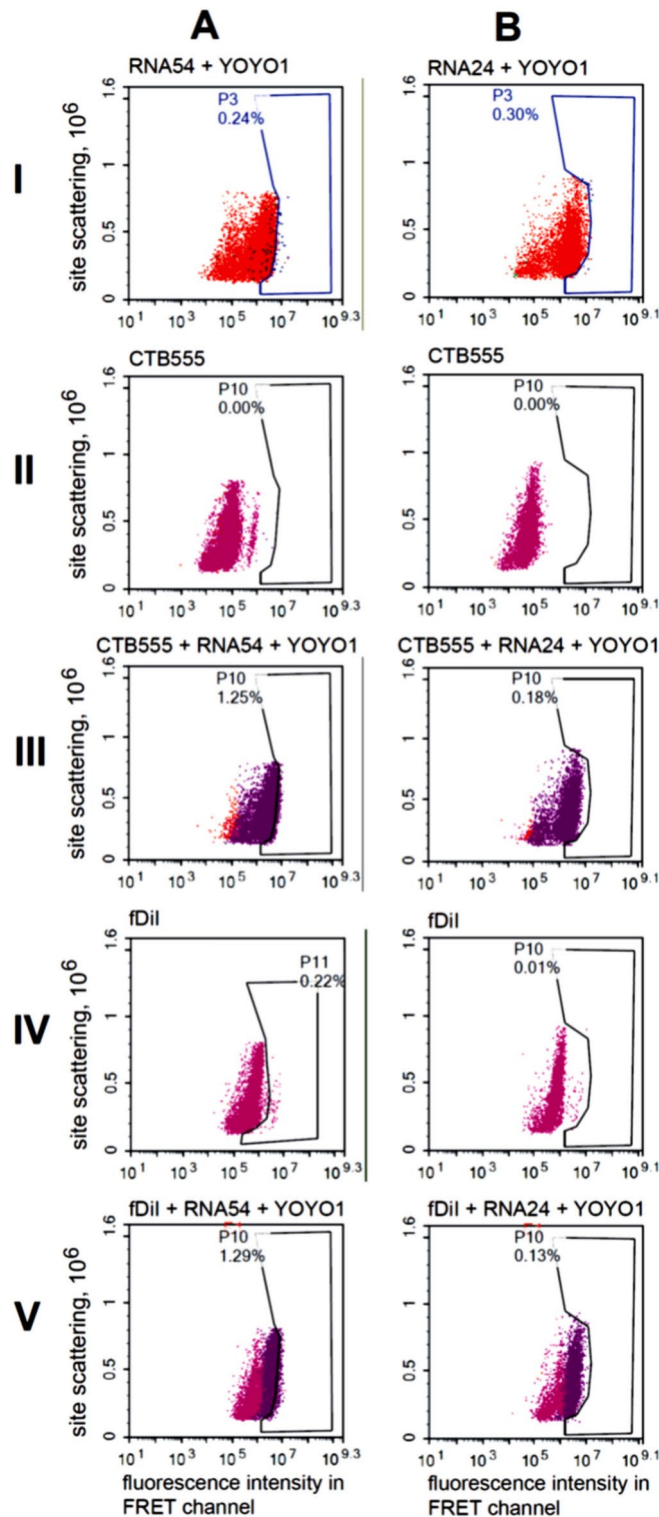
Flow cytometry analysis of RNA aptamers binding to plasma membrane

Figure 3 shows flow cytometry plots for the interaction of RNA 54 (column A) and RNA 24 (column B) with plasma membrane regions in neuroblastoma cells from one representative experiment. The dots represent site scattering (this is a measure of the cellular complexity since light is scattered by the components inside the cells as they pass through the laser beam) vs FRET fluorescence emission signal from cells (bandpass filter [558–586 nm]) with laser excitation at 488 nm. Figures AI and BI (RNA + YOYO-1), AII and BII (CTB555), AIV and BIV (fDiI) show fluorescence emission from single-tagged samples. Panels III and V show the fluorescence emissions from double-tagged samples where FRET occurs between YOYO-1 and CTB555 (row III), or YOYO-1 and fDiI (row V). When the donor (YOYO-1) and the acceptor (CTB555 or fDiI) are sufficiently close, energy transfer occurs from donor to acceptor upon donor excitation, resulting in indirect excitation of CTB555 or fDiI. RNAs are labeled with green YOYO-1, which undergoes a large fluorescent enhancement upon intercalation into RNA structures<sup>23</sup>. YOYO-1 fluorescence indicates the presence of RNA bound to the cell plasma membrane. Cholera toxin B subunit (CTB) attaches to plasma membrane by binding to ganglioside GM1<sup>26</sup>. Neuroblastoma plasma membrane has been labeled with AlexaFluor555 attached to cholera toxin subunit B (CTB555). GM1 molecules strongly partition into rafts<sup>15</sup>, so the orange fluorescence of GM1-bound toxin can be used to visualize lipid rafts within the cell plasma membrane. The fluorescence probe fDiI has been found to preferentially partition into the liquid-disordered phase regions (i.e. outside raft microdomains) of plasma membrane<sup>26–28</sup> therefore the



RNA	54	111	119	13	19	90	145	64	102	24	10	93	20
Apical loop parameter	1.8	2.8	5.3	2.3	1.7	5.0	2.3	2.8	5.3	5.5	3.5	5.0	7.0
% nt in bulge	0%	1%	1%	0%	5%	1%	4%	2%	1%	6%	9%	5%	3%

**Fig. 2.** Average  $K_D$  values for complexes of 13 RNAs with LUV<sub>RAFT</sub> membranes.  $K_D$  values are the mean of 3–4 independent experiments, error bars show a standard error (SEM). Below the graph, the values of the apical loop parameter and % of nucleotides in bulge are given.



orange fluorescence of fDiI indicates the presence of a liquid disordered phase within the neuroblastoma plasma membrane.

Two RNA sequences has been tested (Fig. 3): the strongest membrane binder RNA 54 (apical loop parameter = 1.8, % nt in bulges = 0), and one of the weakest membrane binder RNA 24 (apical loop parameter = 5.5, % nt in bulges = 6). The first row (I) shows the site scattering of the cell vs the fluorescence intensity in FRET channel for unlabeled cells and YOYO-1-labelled RNA 54 (Fig. 3.AI) or YOYO-1-labelled RNA 24 (Fig. 3.BI). This fluorescence is generated by a crosstalk of YOYO-1 (excited at 488 nm) into the FRET region [558–586 nm]. Only 0.24% and 0.30% of the cells falls into the gated region in the case of RNA 54 and RNA 24, respectively. The rows II and IV (Fig. 3) show the site scattering of the cell vs the fluorescence intensity in FRET channel for CTB555 and fDiI labelled cells, respectively, without YOYO-1-labelled RNA. The fluorescence of CTB555 (row

◀ **Fig. 3.** Interaction of selected RNAs with plasma membrane regions measured by flow cytometry of neuroblastoma cells from one representative experiment. Columns A and B represent data for RNA54 and RNA24, respectively. Vertical axis: values of site scattering caused by interrogated cells. Horizontal axis (fluorescence intensity in FRET channel): excitation at 488 nm, emission into a window [558–586] nm due to the FRET YOYO-1 → CTB555 or the FRET YOYO-1 → fDiI. AI (YOYO-1), AII (YOYO-1), BI (CTB555), BII (CTB555), and AIV (fDiI), BIV (fDiI) are single-tagged controls for YOYO-1 labeled RNA, CTB555-labeled cells, and fDiI-labeled cells, respectively. AIII (CTB555), BIII (CTB555), AV (fDiI), BV (fDiI) show the fluorescence emissions from double-tagged cells where FRET is observed between YOYO-1 and CTB555 or between YOYO-1 and fDiI, respectively. YOYO-1 fluorescence indicates the presence of RNA bound to the cell plasma membrane, CTB555 fluorescence indicates the presence of raft microdomains within the cell plasma membrane, and fDiI fluorescence indicates the presence of the liquid disordered phase within the cell plasma membrane. Gated region indicates the population shifted toward higher fluorescence intensity in FRET channel.

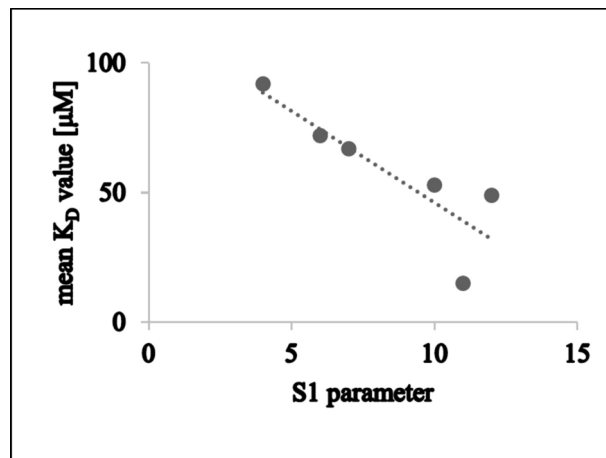


**Fig. 4.** Correlation of  $K_D$  value and S1 parameter for RNA fragments of HTLV-1. S1 parameter is calculated as total number of nucleotides in stems at the apical loop (till the first bulge or internal loop or multi-branch loop) divided by the number of apical loops in a particular RNA molecule ( $n=6$ ). Spearman's correlation coefficient equals  $r_s = -0.94$  (statistically significant for  $p = 0.05$ ). Sequences of RNA fragments were folded using the Mfold program<sup>24</sup> at a set temperature of 37 °C.

II, Fig. 3) does not cross into the FRET region (0% cells fall into the gated region), and the cross talk into the gated region for fDiI is only 0.22% and 0.01% for columns A and B (Fig. 3), respectively.

Gated region indicates the population shifted toward high fluorescence intensity in FRET channel. In the case of RNA 54 (Fig. 3, column I), there is: a five-fold increase in the cell population inside the gated region for CTB-labeled cells (Fig. 3.AII) indicating binding of YOYO-1-labelled RNA 54 to CTB555-labelled lipid raft regions within plasma membrane of neuroblastoma cells, and a four-fold increase (after correction for a crosstalk) in the cell population inside the gated region for fDiI-labeled cells (Fig. 3.AV) indicating the binding of RNA54 also to the non-raft regions of the membrane. In the case of RNA 24 (Fig. 3, column B), there is not any increase in the cell population inside the gated region indicating that RNA 24 does not have any detectable affinity to the membrane, neither to the lipid raft regions nor to the non-raft regions.

### Structural motif analysis of viral RNA fragments

We have generated six short RNA fragments from HTLV-1 RNA, have folded them using both the Mfold and RNAfold programs, have provided alternative structures generated by the Mfold program, have calculated their structural parameters, and have measured the  $K_D$  values of the RNA-RAFT liposome complex (Supplementary Tables S4, S5 and S6). We have performed the correlation analysis between the obtained average  $K_D$  values and structural parameters with the determination of Spearman's correlation coefficient and have tested the statistical significance of Spearman's coefficient for  $p$ -value = 0,05 (Fig. 4 and Supplementary Figure S4).

Figure 4 shows a correlation analysis between the obtained average  $K_D$  values and the S1 parameter for viral RNA fragments. S1 parameter is calculated as total number of nucleotides in stems at the apical loop (till the first bulge or internal loop or multi-branch loop) divided by the number of apical loops in a particular RNA molecule. The calculated Spearman's correlation coefficient is equal to -0.94, with statistical significance for a  $p$ -value of 0.05 ( $n=6$ ). Thus, a strong negative correlation between  $K_D$  value and S1 parameter has been obtained. The negative correlation means that if the value of S1 is higher, the value of  $K_D$  becomes lower. The high value of S1 parameter means the longer double helix at the apical loop. Therefore, the results of the correlation analysis indicate that a long double helix at the apical loop increases the affinity of RNA to lipid rafts. A correlation analysis between the obtained average  $K_D$  values and other structural parameters (including the apical loop



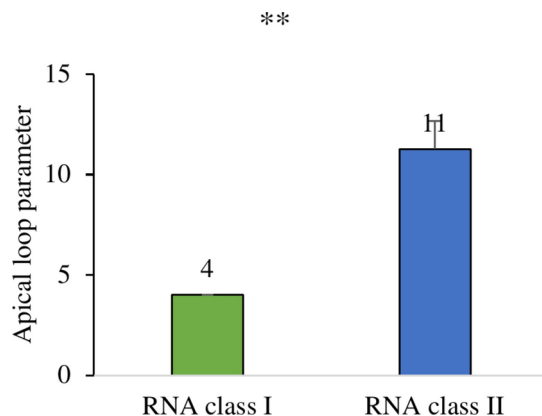


**Fig. 5.** Comparison of an apical loop parameter in two Y RNA classes. The symbol \*\* means that  $p < 0.01$  (Mann–Whitney U test of differences in medians). Error bars show a standard error (SEM). Sequences of Y RNAs were folded using the Mfold program<sup>24</sup> at a set temperature of 37 °C.

parameter and the percentage of nucleotides in stems, bulges, multi-branch loops, apical loops, internal loops, single-stranded terminal regions) shows no statistical significance (Supplementary Figure S4).

### Apical loop parameter in exosomal Y RNAs

In order to estimate whether there is any correlation between the RNA structural motifs and the likelihood of being isolated from exosomes, we have analyzed the apical loop parameter in exosomal Y RNAs. It has been found that exosomes secreted by nematode parasites transfer small RNAs to mammalian cells and modulate innate immunity<sup>29</sup>. In addition to miRNAs, RNAs between 70 and 100 nt were also present in the secreted product, and sequencing identified full-length Y RNAs as the major component of this fraction, with two predominant classes of structure (class I and class II)<sup>29</sup>. Using the Mfold program, the secondary structures of the tested Y RNAs have been predicted (Supplementary Table 7). We have analyzed the structural parameters of four Y RNAs class I (Sanger6, Contig6, Contig11, Sanger7) and eight Y RNAs class II (Contig2, Sanger8, Contig22, Sanger, Contig15, Contig27, HES\_8, Sanger 4, Contig26, Contig19), and we have showed a significant difference in the mean value of apical loop parameter between these two classes. All analyzed Y RNAs contain a RAFT motif (a motif facilitating binding of RNAs to lipid rafts) UCCCU<sup>22</sup>; in addition, Y RNAs from class II contain an EXO motif (a motif that facilitate sorting of miRNAs into exosomes) GGAG<sup>30</sup> and Y RNAs from class I do not contain this motif.

Figure 5 shows a mean values comparison of an apical loop parameter in two Y RNA classes: RNA class I (mean = 4.0) and RNA class II (mean = 11.3). A significant difference between this two groups was confirmed by the Mann–Whitney U test ( $p < 0.01$ ,  $n_{\text{class I}} = 4$ ,  $n_{\text{class II}} = 8$ ). Since the analyzed class I Y RNAs do not contain the EXO motif GGAG, and all the analyzed class II Y RNAs do contain this motif, the presence of the GGAG motif (as the likelihood of being isolated from exosomes) is strongly correlated to the higher value of the apical loop parameter.

### Discussion

The aim of this study was to assess the role of RNA structural motifs in the mechanism of RNA interaction with lipid vesicle membranes. Measurements of the dissociation constant for the interaction of RNAs with membranes of RAFT liposomes were carried out for a panel of RNA oligonucleotides. The obtained  $K_D$  values of the RNA-raft membrane interaction were analyzed for correlations with the structural motifs occurring in the predicted RNA folding.

The results of this study point to a bulge and a small apical loop on a stable stem as potential factors modulating RNA-membrane affinity. A correlation between the RNA-membrane  $K_D$  values and the occurrence of bulges in the RNA structure was obtained, as well as the correlation between  $K_D$  and the calculated parameter indicating the presence of small apical loops in the RNA molecules. On the other hand, the presence of a single-stranded terminal region at the ends of the oligonucleotide molecule may potentially weaken the interaction of RNA with RAFT vesicles. RNA motifs can interact with RNA or protein to influence their functions, e.g. the interactions between RNA loops can lead to a kissing loop complex formation<sup>31</sup>, and the interaction of an RNA bulge and a loop can lead to the formation of a kissing loop/bulge complex<sup>22</sup>. It was also found that the stem structure, the primary sequence of the loop, and the bulge element of the TAR fragment of HIV RNA are the major determinants for Tat protein activation<sup>32</sup>.

Binding of divalent cations to membranes composed of choline bearing phospholipids is weaker when the degree of hydrocarbon chain unsaturation is higher<sup>33</sup> suggesting that calcium and magnesium cations play an important role in the interactions between RNA and membrane domains in liquid-ordered state (lipid rafts). It was suggested<sup>23</sup> that there is a binding interaction between RNA and bilayer head-group dipoles, and that RNA interferes with head-group ordering. The dependence of RNA-raft membrane binding on RNA structure was previously studied in<sup>23</sup>. Although specific membrane-interacting motifs were not identified at that time, a 20-fold change in the percentage of RNA-raft membrane binding was shown to exist depending on changes in RNA

secondary structure. Interestingly, in the same studies, there was no effect of RNA structure modification on the level of binding to DMPC (1,2-dimyristoleoyl-sn-glycero-3-phosphocholine) liposomes localized at the border of the ripple-gel and liquid phases. Similarly, the results of our previous work<sup>22</sup> show that the presence of raft domains in vesicle membranes favors the affinity of RNA oligonucleotides for membranes.

RNA structural elements, including the apical loops, are involved in the regulation of numerous biological processes such as transcription<sup>34</sup>, splicing<sup>35–37</sup>, or RNA transport and processing<sup>38</sup>. The presence of structured regions in RNA molecules promotes the interaction of RNA with many biological molecules, such as RNA-binding proteins (RBPs), ligands, and other RNA types. The complex structure of RNA promotes the formation of stable and well-defined RBP binding sites. Loops and single-stranded RNA regions between double-stranded RNA stems show less conformational flexibility and provide attachment sites for RNA-binding proteins<sup>39</sup>. The importance of the apical loops in binding RNA to various proteins has recently been found: Yb protein involved in primary biogenesis of piRNA<sup>40</sup>, GR protein (glucocorticoid receptor)<sup>41</sup>, one of the transcription factors, and TRIM71 protein<sup>42</sup> involved in cell cycle regulation.

Viral RNA also folds to form secondary and tertiary structures complex enough to enable specific recognition of RNA by proteins during the assembly of viral subunits. RNA structuring is crucial in viral infections in both animals<sup>43</sup> and plants<sup>44</sup>. Apical loop structures also enable long-range ssRNA–ssRNA interactions between RNA molecules. An example is codon-anticodon interactions between mRNA and tRNA, where mRNA bound by the ribosome adopts a loop conformation ready to interact with the anticodon loop of incoming tRNAs<sup>45,46</sup>. In research by Aarum and coworkers<sup>43</sup>, the importance of RNA structure in regulating protein solubility has been identified using synthetic oligonucleotides. Single-stranded pyrimidine-rich bulges or loops surrounded by double-stranded regions were particularly effective in maintaining protein solubility, likely related to maintaining the protein in a functional form<sup>47</sup>.

The influence of RNA structural elements on RNA localization has also been found. For example, <sup>48</sup> found that an apical loop structure serves as a targeting element that directs HAC1 mRNA to the endoplasmic reticulum membrane in yeast. The apical loop structure of RNA associated with the NoRC chromatin remodeling complex is also required for targeting this complex to nucleolar chromatin<sup>49</sup>. An interesting relationship regarding the role of the secondary structure of RNA in its adsorption on flat substrates was also observed by<sup>50</sup>. Researchers found two adsorption systems concerning RNA structure and substrate attraction. With weak surface attraction, base-paired structured RNA fragments attached to the substrate more easily than unstructured RNA fragments (lacking any secondary structure). In turn, increased surface attraction favored the adsorption of unstructured RNA fragments over structured ones. These results suggest selectivity of adsorption between single- and double-stranded RNA regions, highlighting the importance of RNA structure in regulating its adsorption on various substrates.

Regarding RNA interaction with lipid membranes, there are studies that searched for sequence motifs regulating RNA introduction into extracellular vesicles<sup>51,52</sup>. The proposed motifs were present in loop regions of the predicted secondary structures, indicating the potential importance of this structural motif in RNA introduction into vesicles. Conversely, studies on RNA interaction with membranes in the gel phase<sup>53</sup> suggested that RNA binding to membranes depends, among other factors, on the presence of double-stranded structures. Additionally, in the study<sup>54</sup>, where the affinity of RNA fragments containing mRNA localization elements to RAFT vesicles was determined, the highest affinity was observed for RNAs with localization elements in the apical loop structure. This motif's localization likely enables interaction with lipid molecules, thereby increasing RNA affinity for lipid membranes. The literature suggests that RNA interaction with lipid membranes may depend on factors such as RNA nucleotide sequence, secondary structure, or RNA length. The analyses described in this work also suggest that a given RNA's level of affinity for lipid membranes may be regulated by sequence factors (RNA motifs) and structural factors (apical loops). The involvement of secondary structure can also be inferred from the obtained correlation between  $K_D$  values and RNA length or the free energy of molecule folding. The variability of RNA affinity for the membrane appears to be regulated by various factors, including the arrangement of structural and sequential elements and the lipid membrane condition.

The results presented in Fig. 4 indicate that a long double helix at the apical loop in viral RNA fragments increases the affinity of RNA to lipid rafts. It seems that the long double-helix at the loop enables the loop to protrude from the RNA structure and interact with lipid rafts. We have found that the presence of an EXO-motif GGAG in Y RNAs is strongly correlated to the higher value of the apical loop parameter (Fig. 5) suggesting a lower affinity to lipid rafts (Fig. 1). Similar results have been reported for RNA aptamers: RNAs containing an EXO-motif GGAG have been found to exhibit a substantially lower affinity to lipid rafts<sup>22</sup> thus suggesting indirect RNA-exosome interaction via RNA binding proteins<sup>22</sup>. These results indicate that GGAG motif does not enhance direct RNA–membrane interactions but rather is involved in binding of RNA to RBP followed by RBP – membrane interactions. The GGAG sequence was reported to have an affinity to an RBP (hnRNP2B1)<sup>30</sup>.

Difficulties in clear determination of the impact on the level of RNA-membrane interaction of structural motifs may be related to the limitations of the method used to predict the structure of RNA. The secondary structures of RNA proposed by the Mfold program are based on the obtained free energy, calculated with an algorithm focused mainly on Watson–Crick base pairing. This algorithm does not take into account non-canonical nucleotide base pairing, which affects the formation of higher-order RNA structures. For this reason, the actual RNA folding or spatial structure variants may differ from those proposed by the program<sup>55</sup>. In further research, it would also be worth taking into account higher-order structures resulting from non-canonical pairing.

Therapeutic RNAs are used in gene therapy to correct abnormal genes by turning off genes that produce defective proteins or introducing genes to produce a beneficial protein to treat a disease. Being hydrophilic and negatively charged, nucleic acids cannot directly penetrate cell membrane and can be susceptible to enzymatic degradation. Extracellular vesicles such as exosomes can be used as RNA delivery systems that protect nucleic

acids in the bloodstream and deliver them to target sites<sup>56–58</sup>. Our findings demonstrate that RNA structural motifs can be involved in RNA-lipid raft interaction which could contribute to the development of RNA-based lipid biosensors<sup>53</sup> for monitoring of e.g. virus RNAs in biofluids and wastewater<sup>59,60</sup>.

Although several strategies have been proposed to load RNA molecules into exosomes<sup>61</sup>, their efficiency is rather moderate. Moreover, physical methods to load the cargo may compromise the integrity of lipid bilayers that build exosomes, cause aggregation of both vesicles and nucleic acids, and lead to loss of activity of RNAs. Understanding the whole range of factors that regulate RNA interaction with vesicle membranes may further improve methods of efficient loading of the therapeutic RNA into exosomes. RNA binding to vesicle membranes seems to be determined by the arrangement of both structural and sequential elements as well as the condition of the lipid membrane. Future study hopefully help to find a more complete model that could better explain the relationships between these elements and the extent to which they influence the RNA-membrane affinity.

## Materials and methods

### Materials

Lipids: 1,2-dioleoyl-sn-glycero-3-phosphocholine (DOPC); N-stearoyl-D-erythro-sphingosylphosphorylcholine (Stearoyl Sphingomyelin, SM); cholesterol (CHL) were purchased from Avanti Polar Lipids. Fluorescent probes: YOYO<sup>™</sup>-1 Iodide (YOYO-1, 1 mM Solution in DMSO), Lissamine Rhodamine B, 1,2-dihexadecanoyl-sn-glycero-3-phosphoethanolamine triethylammonium salt (LissRh-PE) were purchased from ThermoFisher Scientific. AmpliScribe<sup>™</sup> T7-Flash<sup>™</sup> High Yield Transcription Kit (containing T7 RNA polymerase) was purchased from Lucigen, and PCR set GoTaq<sup>®</sup> PCR Core System I (containing Taq polymerase) was purchased from Promega. IMR-32 neuroblastoma cell line was purchased from the European Collection of Authenticated Cell Cultures (ECACC), a Culture Collection of Public Health England, UK, through Sigma-Aldrich.

### Preparation of large unilamellar vesicles (LUVs)

RAFT liposomes composed of DOPC, SM, and CHL in a molar ratio of 6:3:1 were prepared using the thin-film hydration method followed by extrusion. Appropriate proportions of lipids originally dissolved in chloroform/methanol were mixed, and Lissamine Rhodamine B dye was added (final concentration LissRh-PE = 0.2% mol). Solvents were evaporated under nitrogen gas, and the lipid film was resuspended in warmed (60 °C) RNA Buffer (50 mM HEPES pH 7.0, 50 mM NaCl, 5 mM MgCl<sub>2</sub>, 2 mM CaCl<sub>2</sub>). After incubation at 60 °C for 3 min, multilamellar vesicles (MLVs) were formed by handshaking until complete dissolution. The MLV suspension was subjected to five freeze–thaw cycles followed by vortexing. Large Unilamellar Vesicles (LUVs) were prepared by extrusion using the Avanti MiniExtruder with a filter pore diameter of 100 nm.

### Preparation of RNA aptamers

RNA oligonucleotides were obtained via *in vitro* transcription as described<sup>23,27,54</sup>. The oligonucleotides were 85 to 111 nts in length, including a 50- or 70-nts random region and constant regions at the 5' and 3' ends. The initial RNA pool was generated by T7 polymerase transcription of a DNA template: 5'-TGG TCA TGT GAT CGG CGT ATG—50N or 70N—TAT CGT GTC ATC GTC GTC CCT ATA GTG AGT CGT ATT A-3' (with the T7-promoter region in italics). The original pool of RNA aptamers (148 oligonucleotides)<sup>27</sup> was searched for sequence motifs: EXO-motifs (GGAG, UGAG, CCCU, UCCU)<sup>30</sup> and RAFT-motifs (CCCU, UCCC, CUCC, UUGU)<sup>23,27,54</sup>. Individual RNAs (2.75 μM in highly purified water, 65 °C) were folded by adding 10×RNA buffer, and cooling to room temperature over 10 min before each experimental series.

### Preparation of viral RNA fragments

The sequence of the human T-cell lymphotropic virus type-1 (HTLV-1) have been received from the GenBank database (The National Center for Biotechnology Information, NIH, USA; NCBI Reference Sequence: NC\_001436.1). The following six HTLV-1 RNA fragments have been chosen from different virus RNA regions: V1 fragment (from G6 to G66) from 5'-LTR region, V3 fragment (from G165 to C226) from 5'-LTR region, V38 fragment (from G2777 to G2863) from the coding region, V71 fragment (from G4457 to A4518) from the coding region, V120 fragment (from G7981 to U8042) from the 3'-UTR region, V126 fragment (from G8310 to C 8371) from the 3'-LTR region. These viral RNA fragments have been obtained via *in vitro* transcription as described<sup>23,27,55</sup>. Individual RNAs (2.75 μM in highly purified water, 65 °C) were folded by adding 10×RNA buffer, and cooling to room temperature over 10 min before each experimental series.

### Fluorescent measurements

Fluorescence measurements were performed at room temperature with a constant concentration (0.25 μM) of RNA labelled with YOYO-1 probe (2.5 μM), and increasing lipid concentrations of RAFT liposomes (30 μM—1 mM). RNA-to-membrane FRET (Forster Resonance Energy Transfer) between RNA-bound YOYO-1 (donor) and membrane-bound LissRh-PE (acceptor) was measured by exciting YOYO-1 ( $\lambda_{ex}$  = 483 nm) and monitoring the decrease of its emission intensity ( $\lambda_{em}$  = 511 nm) during titration with RAFT liposomes<sup>22,26,62</sup>. A gradual decrease in YOYO-1 emission fluorescence indicated energy transfer during RNA-membrane interaction.

### K<sub>D</sub> calculations

The K<sub>D</sub> (dissociation constant) of RNA-membrane complex was calculated using the transformed Langmuir isotherm equation. RNA binding data were subjected to nonlinear, least-squares analysis using the Langmuir equation<sup>26,62,63</sup>:  $\Delta F = \Delta F_{max} [x / (K_D + x)]$ , where  $\Delta F_{max}$  is the calculated maximal fluorescence change, x is the vesicle's lipid concentration, and K<sub>D</sub> is the equilibrium dissociation constant for RNA-liposome complexes.



Liposomes without fluorescence probes have been used for correction for light scattering. The  $K_D$  constant is expressed in  $\mu\text{M}$  as the lipid concentration in liposomes at equilibrium (lipids not bound to RNA).

### RNA sequence folding and structural motif search

Sequences of the analyzed RNA oligonucleotides were folded using the Mfold web server in the RNA Institute at the University of Albany<sup>24</sup> at a set temperature of 37 °C. Structural motifs (stem, bulge, multi-branch loop, internal loop, apical loop, and single-stranded terminal region) were marked in the visualizations of the secondary structure with the lowest  $\Delta G$  (Supplementary Table S1). Alternative folds (with lower absolute value of  $\Delta G$ ) for a given sequence are listed in the Supplementary Table S2. RNA sequences were also folded using RNAfold web server in the Institute for Theoretical Chemistry at the University of Vienna<sup>64</sup>.

### Cell culture

IMR-32 cells, a human neuroblastoma cell line, were cultured in Eagle's Minimum Essential Medium (Sigma) supplemented with 1% Non-Essential Amino Acids (NEAA), 2 mM glutamine, 0.5 mg/ml streptomycin sulfate, 100 units/ml penicillin G, and 10% fetal bovine serum (FBS) in a 5% CO<sub>2</sub> and 95% air humidified atmosphere at 37 °C.

### FRET flow cytometry of live neuroblastoma cells

Neuroblastoma IMR-32 cells were prepared for flow cytometry as described<sup>26,28</sup>. Cells were incubated with fDiI or CTB555 at 4 °C for 1 h. Cells were washed twice with HBSS buffer supplemented with 10 mM HEPES and then incubated with YOYO-1-labeled RNA (final concentration 0.25  $\mu\text{M}$ ) at room temperature for 30 min. Cell surface fluorescence was measured using a flow cytometer (NovoCyte, ACEA Biosciences, San Diego, CA, USA). The number of cells analyzed by the cytometer in a single measurement was  $10^4$ . Signals have been measured in the FRET channel also using single-tagged cells for crosstalk correction.

### Statistical analyses

For the obtained values of the dissociation constant  $K_D$  for RNA binding to lipid vesicles, Shapiro–Wilk tests were performed to check the normality of the distribution of the  $K_D$  values. Tests performed at a significance level of 0.05 showed that the distribution of  $K_D$  values did not conform to the normal distribution; therefore, non-parametric tests were used for further statistical analyses. For correlation analyses the one-sided Spearman's rank correlation coefficient was determined and the statistical significance was tested for a p-value of 0.05. Statistical tests were performed in MS Excel, using the Analysis ToolPak and appropriate statistical tables.

### Data availability

The RNA sequences analyzed during the current study are available in the Reference<sup>27</sup> (sequences of RNA aptamers), in the Reference<sup>29</sup> (sequences of Y RNAs), in the Supplementary Table 4 (sequences of viral RNA fragments from HTLV-1), and in the GenBank database—Reference Sequence: NC\_001436.1 (the sequence of viral RNA from HTLV-1).

Received: 7 October 2024; Accepted: 18 February 2025

Published online: 25 February 2025

### References

- Kalluri, R. & LeBleu, V. S. The biology, function, and biomedical applications of exosomes. *Science*. **367**, eaau6977. <https://doi.org/10.1126/science.aau6977> (2020).
- Chung, I. M., Rajakumar, G., Venkidasamy, B., Subramanian, U. & Thiruvengadam, M. Exosomes: Current use and future applications. *Clin. Chim. Acta* **500**, 226–232 (2020).
- Krylova, S. V. & Feng, D. The machinery of exosomes: biogenesis, release, and uptake. *Int. J. Mol. Sci.* **24**, 1337. <https://doi.org/10.3390/ijms24021337> (2023).
- Valadi, H. et al. Exosome-mediated transfer of mRNAs and microRNAs is a novel mechanism of genetic exchange between cells. *Nat. Cell Biol.* **9**, 654–659 (2007).
- Pitt, J. M. et al. Dendritic cell-derived exosomes as immunotherapies in the fight against cancer. *J. Immunol.* **193**, 1006–1011 (2014).
- Xu, R., Greening, D. W., Zhu, H. J., Takahashi, N. & Simpson, R. J. Extracellular vesicle isolation and characterization: Toward clinical application. *J. Clin. Investig.* **126**, 1152–1162 (2016).
- Turchinovich, A., Toneyvitsky, A. G. & Burwinkel, B. Extracellular miRNA: A collision of two paradigms. *Trends Biochem. Sci.* **41**, 883–892 (2016).
- Hu, W. et al. Comprehensive land-scape of extracellular vesicle-derived RNAs in cancer initiation, progression, metastasis and cancer immunology. *Mol. Cancer* **19**, 102. <https://doi.org/10.1186/s12943-020-01199-1> (2020).
- Darband, S. G. et al. Exosomes: natural nanoparticles as bio shuttles for RNAi delivery. *J. Control. Release* **289**, 158–170 (2018).
- Rajagopal, C. & Harikumar, K. B. The origin and functions of exosomes in cancer. *Front. Oncol.* **8**, 66. <https://doi.org/10.3389/fonc.2018.00066> (2018).
- Trajkovic, K. et al. Ceramide triggers budding of exosome vesicles into multivesicular endosomes. *Science* **319**, 1244–1247 (2008).
- Janas, T., Janas, M. M., Sapoń, K. & Janas, T. Mechanisms of RNA loading into exosomes. *FEBS Lett.* **589**, 1391–1398 (2015).
- Anand, S., Samuel, M., Kumar, S. & Mathivanan, S. Ticket to a bubble ride: Cargo sorting into exosomes and extracellular vesicles. *Biochim. Biophys. Acta Prot. Proteom.* **1867**, 140203. <https://doi.org/10.1016/j.bbapap.2019.02.005> (2019).
- Sapoń, K., Mańka, R., Janas, T. & Janas, T. The role of lipid RAFTs in vesicle formation. *J. Cell Sci.* **136**, jcs260887. <https://doi.org/10.1242/jcs.260887> (2023).
- Pike, L. J. RAFTs defined: A report on the Keystone Symposium on Lipid RAFTs and Cell Function. *J. Lipid Res.* **47**, 1597–1598 (2006).
- Kaiser, H. J. et al. Order of lipid phases in model and plasma membranes. *Proc. Natl. Acad. Sci. USA* **106**, 16645–16650 (2009).
- Simons, K. & Ikonen, E. Functional RAFTs in cell membranes. *Nature* **387**, 569–572 (1997).
- Dietrich, C. et al. Lipid rafts reconstituted in model membranes. *Biophys. J.* **80**, 1417–1428 (2001).

19. Hirano, K., Kinoshita, M. & Matsumori, N. Impact of sphingomyelin acyl chain heterogeneity upon properties of RAFT-like membranes. *Biochim. Biophys. Acta Biomembr.* **1864**, 184036. <https://doi.org/10.1016/j.bbmem.2022.184036> (2022).
20. Rivas, M. & Fox, G. E. Nonstandard RNA/RNA interactions likely enhance folding and stability of segmented ribosomes. *RNA* **28**, 340–352 (2022).
21. Flores, J. K. & Ataide, S. F. Structural changes of RNA in complex with proteins in the SRP. *Front. Mol. Biosci.* **5**, 7. <https://doi.org/10.3389/fmolb.2018.00007> (2018).
22. Mańka, R., Janas, P., Sapoń, K., Janas, T. & Janas, T. Role of RNA motifs in RNA interaction with membrane lipid rafts: implications for therapeutic applications of exosomal RNAs. *Int. J. Mol. Sci.* **22**, 9416. <https://doi.org/10.3390/ijms22179416> (2021).
23. Janas, T., Janas, T. & Yarus, M. Specific RNA binding to ordered phospholipid bilayers. *Nucl. Acids Res.* **34**, 2128–2136 (2006).
24. Zuker, M. Mfold web server for nucleic acid folding and hybridization prediction. *Nucl. Acids Res.* **31**, 3406–3415 (2003).
25. Tinoco, I. Jr. & Bustamante, C. How RNA folds. *J. Mol. Biol.* **293**, 271–281 (1999).
26. Sapoń, K., Janas, T., Sikorski, A. F. & Janas, T. Polysialic acid chains exhibit enhanced affinity for ordered regions of membranes. *Biochim. Biophys. Acta Biomembr.* **1861**, 245–255 (2019).
27. Janas, T., Janas, P., Sapoń, K. & Janas, T. Binding of RNA aptamers to membrane lipid rafts: implications for exosomal miRNAs transfer from cancer to immune cells. *Int. J. Mol. Sci.* **21**, 8503. <https://doi.org/10.3390/ijms21228503> (2020).
28. Janas, T., Sapoń, K. & Janas, T. Selection of bifunctional RNAs with specificity for arginine and lipid membranes. *FEBS Lett.* **598**, 1061–1079 (2024).
29. Buck, A. H. et al. Exosomes secreted by nematode parasites transfer small RNAs to mammalian cells and modulate innate immunity. *Nat. Commun.* **5**, 5488. <https://doi.org/10.1038/ncomms6488> (2014).
30. Villarroya-Beltri, C. et al. Sumoylated hnRNP A2B1 controls the sorting of miRNAs into exosomes through binding to specific motifs. *Nat. Commun.* **4**, 2980. <https://doi.org/10.1038/ncomms3980> (2013).
31. Vlassov, A., Khvorova, A. & Yarus, M. Binding and disruption of phospholipid bilayers by supramolecular RNA complexes. *Proc. Natl. Acad. Sci. USA* **98**, 7706–7711 (2001).
32. Wu, F., Garcia, J., Sigman, D. & Gaynor, R. Tat regulates binding of the human immunodeficiency virus trans-activating region RNA loop-binding protein TRP-185. *Genes Dev.* **5**, 2128–2140 (1991).
33. Lis, L. J., Lis, W. T., Parsegian, V. A. & Rand, R. P. Adsorption of divalent cations to a variety of phosphatidylcholine bilayers. *Biochemistry* **20**, 1771–1777 (1981).
34. Kozak, M. Regulation of translation via mRNA structure in prokaryotes and eukaryotes. *Gene* **361**, 13–37 (2005).
35. Jacobs, E., Mills, J. D. & Janitz, M. The role of RNA structure in posttranscriptional regulation of gene expression. *J. Genet. Genom.* **39**, 535–543 (2012).
36. Bartys, N., Kierzek, R. & Lisowiec-Wachnicka, J. The regulation properties of RNA secondary structure in alternative splicing. *Biochim. Biophys. Acta Gene Regul. Mech.* **1862**, 194401. <https://doi.org/10.1016/j.bbagr.2019.07.002> (2019).
37. Taylor, K. & Sobczak, K. Intrinsic regulatory role of RNA structural arrangement in alternative splicing control. *Int. J. Mol. Sci.* **21**, 5161. <https://doi.org/10.3390/ijms21145161> (2020).
38. Lazzaretti, D. & Bono, F. mRNA localization in metazoans: A structural perspective. *RNA Biol.* **14**, 1473–1484 (2017).
39. Armaos, A., Zacco, E., de Groot, N. S. & Tartaglia, G. G. RNA-protein interactions: Central players in coordination of regulatory networks. *BioEssays* **43**, 2000118. <https://doi.org/10.1002/bies.202000118> (2021).
40. Takase, N. et al. T-hairpin structure found in the RNA element involved in piRNA biogenesis. *RNA* **28**, 541–550 (2022).
41. Hörberg, J. & Reymer, A. Decoding the dual recognition mechanism of the glucocorticoid receptor for DNA and RNA: sequence versus shape. *Sci. Rep.* **13**, 16125. <https://doi.org/10.1038/s41598-023-43244-1> (2023).
42. Shi, F. et al. Molecular mechanism governing RNA-binding property of mammalian TRIM71 protein. *Sci. Bull.* **69**, 72–81 (2024).
43. Ye, L. et al. RNA structures and their role in selective genome packaging. *Viruses* **13**, 1788. <https://doi.org/10.3390/v13091788> (2021).
44. Wu, J., Leontis, N. B., Zirbel, C. L., Bisaro, D. M. & Ding, B. A three-dimensional RNA motif mediates directional trafficking of Potato spindle tuber viroid from epidermal to palisade mesophyll cells in *Nicotiana benthamiana*. *PLoS Pathog.* **15**, e1008147. <https://doi.org/10.1371/journal.ppat.1008147> (2019).
45. Grosjean, H. & Westhof, E. An integrated, structure-and energy-based view of the genetic code. *Nucl. Acids Res.* **44**, 8020–8040 (2016).
46. Skeparnias, I. & Zhang, J. Cooperativity and interdependency between RNA structure and RNA–RNA interactions. *Non-coding RNA* **7**, 81. <https://doi.org/10.3390/ncrna7040081> (2021).
47. Aarum, J. et al. Enzymatic degradation of RNA causes widespread protein aggregation in cell and tissue lysates. *EMBO reports* **21**, e49585. <https://doi.org/10.15252/embr.201949585> (2020).
48. Aragón, T. et al. Messenger RNA targeting to endoplasmic reticulum stress signalling sites. *Nature* **457**, 736–740 (2009).
49. Mayer, C., Neubert, M. & Grummt, I. The structure of NoRC-associated RNA is crucial for targeting the chromatin remodelling complex NoRC to the nucleolus. *EMBO Rep.* **9**, 774–780 (2008).
50. Poblete, S., Bozic, A., Kanduc, M., Podgornik, R. & Guzman, H. V. RNA secondary structures regulate adsorption of fragments onto flat substrates. *ACS omega* **6**, 32823–32831 (2021).
51. Batagov, A. O., Kuznetsov, V. A. & Kurochkin, I. V. Identification of nucleotide patterns enriched in secreted RNAs as putative cis-acting elements targeting them to exosome nano-vesicles. *BMC Genom.* <https://doi.org/10.1186/1471-2164-12-S3-S18> (2011).
52. Bolukbasi, M. F. et al. miR-1289 and “Zipcode”-like sequence enrich mRNAs in microvesicles. *Mol. Ther. Nucl. Acids* **1**, e10. <https://doi.org/10.1038/mtna.2011.2> (2012).
53. Czerniak, T. & Saenz, J. P. Lipid membranes modulate the activity of RNA through sequence-dependent interactions. *Proc. Natl. Acad. Sci. USA* **119**, 2119235119. <https://doi.org/10.1073/pnas.2119235119> (2022).
54. Janas, T., Sapoń, K., Janas, T. & Yarus, M. Specific binding of VegT mRNA localization signal to membranes in *Xenopus* oocytes. *Biochim. Biophys. Acta Mol. Cell Res.* **1868**, 118952. <https://doi.org/10.1016/j.bbmc.2021.118952> (2021).
55. Vicens, Q. & Kieft, J. S. Thoughts on how to think (and talk) about RNA structure. *Proc. Natl. Acad. Sci. USA* **119**, e2112677119. <https://doi.org/10.1073/pnas.2112677119> (2022).
56. Rezaei, R. et al. Exosome-mediated delivery of functionally active miRNA-375–3p mimic regulate epithelial mesenchymal transition (EMT) of colon cancer cells. *Life Sci.* **269**, 119035. <https://doi.org/10.1016/j.lfs.2021.119035> (2021).
57. Li, Z. et al. Non-small-cell lung cancer regression by siRNA delivered through exosomes that display EGFR RNA aptamer. *Nucl. Acid Ther.* **31**, 364–374 (2021).
58. Zhang, Y. et al. Recent advances in exosome-mediated nucleic acid delivery for cancer therapy. *J. Nanobiotechnol.* **20**, 279. <https://doi.org/10.1186/s12951-022-01472-z> (2022).
59. Kamat, S., Kumari, M. & Jayabaskaran, C. Nano-engineered tools in the diagnosis, therapeutics, prevention, and mitigation of SARS-CoV-2. *J. Control. Release* **338**, 813–836. <https://doi.org/10.1016/j.jconrel.2021.08.046> (2021).
60. Selivanovitch, E., Ostwalt, A., Chao, Z. & Daniel, S. Emerging Designs and Applications for Biomembrane Biosensors. *Annu. Rev. Anal. Chem.* **17**, 339–366. <https://doi.org/10.1146/annurev-anchem-061622-042618> (2024).
61. Lu, Y., Huang, W., Li, M. & Zheng, A. Exosome-Based Carrier for RNA Delivery: Progress and Challenges. *Pharmaceutics* **15**, 598. <https://doi.org/10.3390/pharmaceutics15020598> (2023).
62. Janas, T., Janas, T. & Yarus, M. A membrane transporter for tryptophan composed of RNA. *RNA* **10**, 1541–1549 (2004).
63. Sapoń, K., Gawrońska, I., Janas, T., Sikorski, A. F. & Janas, T. Exosome-associated polysialic acid modulates membrane potentials, membrane thermotropic properties, and RAFT-dependent interactions between vesicles. *FEBS Lett.* **594**, 1685–1697 (2020).

64. Gruber, A. R., Lorenz, R., Bernhart, S. H., Neuböck, R. & Hofacker, I. L. The Vienna RNA Websuite. *Nucl. Acids Res.* **36**, W70–W74. <https://doi.org/10.1093/nar/gkn188> (2008).

## Acknowledgements

The authors thank prof. Michael Yarus (University of Colorado at Boulder) for inspiring discussions.

## Author contributions

R.M., K.S. J.Z. performed data acquisition. R.M., K.S. carried out data analysis; R.M., Ter.J., Tad.J. conceived the study. Tad.J. supervised the study. Tad.J., A.C. provided resources. R.M., K.S., Ter.J., A.C., Tad.J. wrote the manuscript.

## Funding

This work was supported by the National Science Centre, Poland, Grant no. 2016/23/B/NZ1/02975.

## Declarations

## Competing interests

The authors declare no competing interests.

## Additional information

**Supplementary Information** The online version contains supplementary material available at <https://doi.org/10.1038/s41598-025-91093-x>.

**Correspondence** and requests for materials should be addressed to T.J.

**Reprints and permissions information** is available at [www.nature.com/reprints](http://www.nature.com/reprints).

**Publisher's note** Springer Nature remains neutral with regard to jurisdictional claims in published maps and institutional affiliations.

**Open Access** This article is licensed under a Creative Commons Attribution-NonCommercial-NoDerivatives 4.0 International License, which permits any non-commercial use, sharing, distribution and reproduction in any medium or format, as long as you give appropriate credit to the original author(s) and the source, provide a link to the Creative Commons licence, and indicate if you modified the licensed material. You do not have permission under this licence to share adapted material derived from this article or parts of it. The images or other third party material in this article are included in the article's Creative Commons licence, unless indicated otherwise in a credit line to the material. If material is not included in the article's Creative Commons licence and your intended use is not permitted by statutory regulation or exceeds the permitted use, you will need to obtain permission directly from the copyright holder. To view a copy of this licence, visit <http://creativecommons.org/licenses/by-nc-nd/4.0/>.

© The Author(s) 2025